Adolescent Thalamocortical Inhibition Alters Prefrontal Excitation-Inhibition Balance

David Petersen[1,3], Christoph Kellendonk[1,2,3,#], Sarah Canetta[1,4,#],

[1]Department of Psychiatry, [2]Department of Molecular Pharmacology & Therapeutics, Vagelos College of Physicians and Surgeons, Columbia University Irving Medical Center, New York, NY 10032, USA

[3]Division of Molecular Therapeutics, [4]Division of Developmental Neuroscience, , New York State Psychiatric Institute, New York, NY, 10032

[#]Equal contribution

*Correspondence: ck491@cumc.columbia.edu, ses2119@cumc.columbia.edu

Abstract

Adolescent inhibition of thalamo-cortical projections leads to long lasting deficits in prefrontal cortex function and cognition in the adult mouse. While this suggests a role of thalamic activity in prefrontal cortex maturation, it is unclear how inhibition of these projections affects prefrontal network function during adolescence. Here, we used chemogenetic tools to inhibit thalamo-prefrontal projections in the mouse from postnatal day 20-35 and measured synaptic inputs to prefrontal pyramidal neurons by layer (either II/III or V/VI) and projection target twenty-four hours later using slice physiology. We found a decrease in the frequency of excitatory and inhibitory currents in layer II/III nucleus accumbens projecting and layer V/VI mediodorsal thalamus projecting neurons. In contrast, layer V/VI nucleus accumbens projecting neurons showed an increase in the amplitude of excitatory and inhibitory currents. In addition, the frequency of inhibitory currents in contralateral mPFC projecting neurons was also enhanced. Notably, despite these complex changes in individual levels of excitation and inhibition, the overall balance between excitation and inhibition was only changed in cortico-cortical projections. This finding suggests homeostatic regulation occurs within subcortically- but not cross-hemispheric intracortical projecting neurons, increased inhibition of intra-prefrontal connectivity may therefore be particularly important for prefrontal cortex circuit maturation.

Keywords

Adolescence, Excitation-inhibition balance, Thalamocortical projections, Prefrontal cortex maturation

47 **Introduction**

48 The prefrontal cortex (PFC) supports high level cognitive functioning including working
49 memory and other executive functions (Fuster, 2001; Miller et al., 2018). An impairment in
50 the development or maturation of the prefrontal cortex during adolescence has been postulated to
51 contribute to the cognitive deficits observed in patients with schizophrenia (Feinberg, 1982;
52 Weinberger, 1987; Paus et al., 2008; Gogtay et al., 2011; Rapoport et al., 2012; Sakurai and
53 Gamo, 2019; Chini and Hanganu-Opatz, 2021; Dienel et al., 2022; Smucny et al., 2022).
54 Thalamic inputs regulate sensory cortical maturation during sensitive time windows of
55 development (Wiesel and Hubel, 1963; Nabel and Morishita, 2013; Benoit et al., 2022a). We
56 recently established in the mouse that thalamic input activity during adolescence is necessary for
57 adult prefrontal cortex function and behavior (Benoit et al., 2022b). More specifically, we found
58 that decreasing activity in the mediodorsal thalamus from postnatal day 20-50 using
59 pharmacogenetic tools led to deficits in the performance of two prefrontal dependent cognitive
60 tasks addressing working memory and attentional set shifting. These deficits were measured in
61 the adult mouse and associated with decreased anatomical thalamocortical projections and
62 decreased functional excitatory post-synaptic currents measured in layer 2/3 prefrontal cortical
63 pyramidal cells. Moreover, mice with thalamic inhibition during adolescence showed decreased
64 correlated activity between neurons in the prefrontal cortex while performing an attentional set
65 shifting task and the ability of the prefrontal cortex to decode task outcomes was impaired
66 (Benoit et al., 2022b). Notably, decreasing the activity of thalamocortical projections for a
67 comparable length period in adulthood, did not lead to the same long-lasting effects.
68

69 These findings established that thalamo-prefrontal activity is required during adolescence to
70 sustain normal thalamocortical connectivity, prefrontal network function, and cognitive behavior
71 in adulthood. However, it was not clear whether these effects on circuit connectivity were
72 apparent immediately following the adolescent manipulation or require maturation into
73 adulthood to manifest. Moreover, it was not clear whether the main impact of decreased
74 adolescent thalamo-prefrontal activity on prefrontal cortical circuitry is to reduce excitatory
75 thalamic afferents or whether this manipulation leads to more widespread changes in the intrinsic
76 connectivity of this brain region.
77
78 To address these questions, we undertook a detailed study of prefrontal cortical connectivity
79 using slice electrophysiology twenty-four hours following pharmacogenetic inhibition of
80 thalamo-prefrontal projections from postnatal day P20-35. We chose this reduced window of
81 inhibition because: 1) Prior work demonstrated changes in the density of thalamic projections to
82 the PFC following adolescent thalamocortical inhibition are already present at this time (Benoit
83 et al., 2022b) and 2) Unpublished work from our laboratory established that inhibiting thalamo-
84 prefrontal projections in this window is sufficient to induce lasting effects on cognitive behavior
85 in adulthood. We first recorded excitatory and inhibitory currents from layer II/III neurons as
86 previously done in the adult (Benoit et al., 2022b), to establish whether the previously observed
87 deficit arises during adolescence. We then restricted our recordings to specific mPFC projection
88 neurons identified by their projection target and cortical layer. We found excitatory post synaptic
89 currents are already reduced in layer II/III cells during adolescence, as in adult mice. When
90 analyzing specific projections, we found a reduction in frequency of excitatory and inhibitory
91 currents in layer V/VI cortico-thalamic cells and layer II/III cortico-accumbens projecting cells

while layer V/VI cortico-accumbens projecting neurons displayed increased amplitudes of excitatory and inhibitory currents. While we observed changes in the absolute frequency of excitatory or inhibitory inputs in all these subcortically projecting cells following adolescent thalamic inhibition, notably the overall balance of excitatory and inhibitory currents experienced by a given cell was not affected, suggesting homeostatic mechanisms may offset decreased excitatory inputs. In contrast, in cross-hemispheric cortico-cortical projection neurons, we observed a significant increase in the frequency of inhibitory inputs, and no change in excitatory inputs, following adolescent thalamic inhibition, with a significant decrease in the overall ratio of the frequency of excitatory to inhibitory currents. Together, these data show a complex adaptation of cortical network activity in response to decreased thalamocortical activity during adolescence and suggest that activity in cells projecting to contralateral PFC may be most profoundly affected due to a lack of homeostatic adaptation.

Materials and Methods

Animal Husbandry

All procedures were performed in accordance with guidelines approved by the Institutional Animal Care and Use Committees at Columbia University and the New York State Psychiatric Institute (protocol NYSPI 1589). Animals were housed under a 12-h light/12-h dark cycle in a temperature-controlled environment (22 °C, humidity of 30–70%) with food and water available ad libitum, unless otherwise noted. C57/ BL6 females and males (Jackson Laboratories, 000664) were used for all experiments. Littermates were randomly assigned to each experimental group, with random distribution across males and females. Mice were housed together with dams and littermates. Offspring were weaned at P28, and

115 group housed with same-sex littermates (no more than five mice per cage). For thalamic
116 inhibition, mice were given intraperitoneal (i.p.) injections of JHU37160 (J60, a CNO
117 analog) dissolved in 0.9% sterile saline at 0.1 mg/kg twice per day (Bonaventura et al., 2019).
118 J60 was used as an alternative to the widely used clozapine-N-oxide (CNO) because J60 is
119 known to have less off-target effects. New evidence has shown CNO might be reverse
120 metabolized into clozapine, a common antipsychotic medication with high affinity to
121 dopamine D2 and serotonin 2A receptors (Manvich et al., 2018). All mice were given J60
122 regardless of viral vector, except those given saline with hM4D expression. Surgeries were
123 conducted at P12-13, and all mice were injected from P20 to P35. 24 hours after the final
124 J60 injection, P35 (+/- 4 days), mice were anesthetized with isoflurane and decapitated for
125 slice electrophysiology. Throughout data collection and analysis, experimenters were
126 blinded to the group of the animal. For the dual virus approach, C57/BL6 males and females
127 were bred, and littermates were used for the experiment. We based sample sizes on previous
128 experiments, and no statistical methods were used to calculate sample sizes.
129

130 **Surgical Procedures**

131 For viral injections at P13, mice were anesthetized with isoflurane, and head-fixed in a
132 stereotactic apparatus (Kopf). Mice were injected bilaterally in the midline thalamus with
133 AAV5-hSyn-DIO-hM4D-mCherry (Addgene, 44362) or a control virus, AAV5-hSyn-DIO-
134 mCherry (Addgene, 50459), at a volume of 0.25 µl (0.1µl/min). Mice were also injected
135 bilaterally in the mPFC with retrograde AAV-hSyn-Cre-WPRE-hGH (Addgene, 105553) at a
136 volume of 0.2 µl (0.1 µl/min). For the tracer experiments mice were injected with retrograde
137 AAV-hSyn-EGFP (Addgene, 50465) at a volume of 0.25 µl for the MD, 0.2 µl for the mPFC, and

138 0.1µl for the NAc. The following were the P13 coordinates: MD thalamus, −0.85 anterior–
139 posterior (AP), ±0.20 medial–lateral (ML) and −3.25 dorsal–ventral (DV, zero at brain surface);
140 mPFC, 2.4 AP, ±0.2 ML and −1.9 DV (zero at brain surface); NAc, 1.7 AP, ±1.1 ML and −5.07
141 DV. All coordinates were zeroed at bregma unless otherwise noted.
142

143 **Slice Electrophysiology**

144 Whole-cell voltage clamp recordings were performed in layer II/III mPFC pyramidal cells
145 and layer V/VI mPFC pyramidal cells. Recordings were obtained with a Multiclamp 700B
146 amplifier (Molecular Devices) and digitized using a Digidata 1440B acquisition system
147 (Molecular Devices) with Clampex 10 (Molecular Devices) and analyzed with pClamp 10
148 (Molecular Devices). Following decapitation, 300-µm slices containing mPFC were
149 incubated in artificial cerebral spinal fluid containing 126mM NaCl, 2.5mM KCl, 2.0mM
150 MgCl2, 1.25mM NaH2PO4, 2.0mM CaCl2, 26.2mM NaHCO3 and 10.0mM d-glucose (pH
151 7.45, 310 mOsm) bubbled with oxygen at 32 °C for 30min before being returned to room
152 temperature for at least 1 hour before use. During recording, slices were perfused in room
153 temperature artificial cerebral spinal fluid at a rate of 5 ml/min. Electrodes were pulled from
154 1.5-mm borosilicate glass pipettes on a P-97 puller (Sutter Instruments). Electrode
155 resistance was typically 1.5–3MΩ when filled with internal solution consisting of 130mM
156 cesium hydroxide monohydrate, 130mM D-gluconic acid, 10mM HEPES, 2.0mM MgCL2,
157 0.2mM EGTA, 2.5mM Mg-ATP, 0.3mM Na-GTP, and 5mM Lidocaine N-ethyl bromide (pH
158 7.3, 277mOsm).
159 *mPFC recordings.* Animals were sacrificed for recordings at P35 after adolescent
160 manipulation. mPFC pyramidal cells were visually identified based on their shape and

161 prominent apical dendrite at ×40 magnification under infrared and diffusion interference
162 contrast microscopy. Recordings were taken from either layer II/III of the mPFC (PrL) or
163 layer V/VI. Layer II/III was defined as any cell lying 150µm-350µm from the pial surface.
164 Layer V/VI was defined as cells within 400µm-600µm from the pial surface. Spontaneous
165 excitatory post synaptic currents (sEPSCs) were recorded in voltage clamp at a holding
166 potential of −65mV, and spontaneous inhibitory post-synaptic currents (sIPSCs) were
167 recorded in voltage clamp at a holding potential of +10mV; 60 s of the current recording for
168 each condition was analyzed. Recordings were filtered with a 2 kHz eight-pole low-pass
169 Bessel filter, and sEPSCs and sIPSCs were detected using MiniAnalysis (Synaptosoft).
170 Frequency, amplitude, and instantaneous frequency were calculated for all traces. Frequency
171 was calculated by dividing the total number of events by time (60s). Amplitude was the
172 distance from baseline to the tip of the event. Instantaneous frequency was the inverse of the
173 interevent-interval converted to a frequency. All event data were averaged by cell.
174

175 **Statistics**

176 Statistical analysis and graph preparations were done using Prism 9 software (GraphPad
177 Software), JASP (JASP Team (2023), JASP (Version 0.17.3) or custom scripts in R. Linear
178 mixed effects models with individual animal used as a random-effects grouping factor were
179 used to analyze slice physiology. Linear mixed effects models were used over a common
180 ANOVA or t-test to account for the possible non-independence of measurements from cells
181 from the same animal. Outliers were removed using the following equation Q1-1.5 x IQR or
182 Q3 + 1.5 x IQR, this corresponds to +/- 2.698σ from the mean. For the nonspecific L II/III
183 experiment, 2 outliers were removed from the EPSC hM4D+Saline amplitude group, 1

184 outlier was removed from the IPSC hM4D frequency group, and 1 outlier was removed from
185 the IPSC hM4D instantaneous frequency group. For the cortico-accumbens experiment, 2
186 outliers were removed from the IPSC hM4D group. For the cortico-cortical population
187 experiment, 2 outliers were removed from the IPSC mCherry frequency group. For the E/I
188 balance analysis, 2 outliers were removed from the hM4D cortico-cortical frequency group.
189

190 **Results**

191 **Adolescent thalamocortical activity regulates excitatory transmission to**
192 **superficial mPFC.**

193 We first performed patch clamp recordings in brain slices from prelimbic layer II/III neurons,
194 which is the mPFC population of projection neurons that obtain the most prominent input from
195 the MD (Anastasiades and Carter, 2021). To inhibit thalamic activity during adolescence on
196 postnatal day 13 (P13), we injected an adeno-associated virus (AAV) carrying a Cre-dependent
197 version of the inhibitory designer receptor hM4D into the thalamus of C57 mice and a retrograde
198 virus, rgAAV-CRE, into the mPFC. Retrograde transport will cause Cre recombinase expression
199 in the MD leading to hM4D expression selectively in medial prefrontal projecting neurons (Fig.
200 1a). We then chronically inhibited these cortically projecting MD cells with the hM4D ligand
201 JHU37160 (J60) (0.1 mg/kg) from postnatal day 20 until the day before they were recorded
202 (P35(-4days)) (Fig. 1b). To control for the possible non-ligand-dependent effects of the hM4D
203 receptor, we also included a group of mice expressing hM4D that were injected with saline
204 during the same developmental window. Twenty-four hours after the last J60 injection (at
205 P35±4days), we recorded layer II/III neurons and analyzed excitatory and inhibitory post-
206 synaptic currents.

Using linear mixed effects models, we found that inhibition of thalamocortical projections from P20-35 decreased the frequency [$F(2, 5.93) = 6.854$, $p = 0.029$] and spatial distribution (instantaneous frequency) [$F(1,7.02) = 8.129$, $p = 0.025$] of spontaneous excitatory currents (sEPSCs), while there was no change in the amplitude [$F(2, 42) = 1.763$, $p = 0.184$] of sEPSCs when compared to controls (Fig. 1f-i). Measuring spontaneous inhibitory currents (sIPSCs) resulted in a trend of diminished frequency [$F(2, 9.78) = 2.906$, $p = 0.102$] while spatial distribution (instantaneous frequency) [$F(2, 10.92) = 1.973$, $p = 0.185$] and amplitude [$F(2, 8.41) = 0.458$, $p = 0.458$] remained unchanged when compared to controls (Fig. 1f-i). Furthermore, when comparing the mCherry and Saline groups in a post-hoc contrast, no significant differences were observed, signaling the lack of non-ligand dependent effects of the hM4D receptor (EPSC frequency [$z(\infty) = 0.501$, $p_{\text{bonferroni}} = 1.000$]; EPSC median instantaneous frequency [$z(\infty) = 1.097$, $p_{\text{bonferroni}} = 0.818$]; and no overall effect in EPSC amplitude, IPSC frequency, IPSC instantaneous frequency, or IPSC amplitude. These results indicate that adolescent thalamocortical activity causes significant alterations to excitatory transmission in the superficial regions of the mPFC, consistent with what we previously found in adult mice. (Benoit et al., 2022b).

Adolescent thalamocortical activity regulates excitatory and inhibitory transmission to superficial layer II/III cortico-accumbens projections.

We then determined whether the observed effects of adolescent thalamocortical inhibition includes the layer II/III cortico-accumbens cell populations. To this end, we injected the rgGFP virus into the nucleus accumbens (NAc) (Fig. 2a-b) and recorded from the superficial layers (II/III) of the mPFC. We found that in superficial NAc-projecting neurons, excitatory and inhibitory transmission were both dampened following adolescent thalamocortical inhibition. For

230 excitatory currents, the frequency [$F(1, 47) = 9.354$, $p = 0.004$] was significantly decreased but
231 not the spatial distribution (instantaneous frequency) [$F(1, 6.77) = 1.926$, $p = 0.208$] or the
232 amplitude [$F(1, 6.19) = 3.313$, $p = 0.117$] (Fig. 2e-f). For inhibitory transmission in superficial
233 layers, sIPSC frequency was reduced [$F(1, 4.89) = 9.451$, $p = 0.028$] but not the spatial
234 distribution (instantaneous frequency) [$F(1, 7.79) = 0.955$, $p = 0.358$] or the amplitude [$F(1, 7.03)$
235 $= 3.402$, $p = 0.107$] (Fig. 2g-h). These data show that excitatory and inhibitory inputs are
236 decreased onto layer II/III accumbens projecting neurons.
237

238 **Adolescent thalamocortical activity regulates excitatory and inhibitory**
239 **transmission to cortico-thalamic projections.**

240 We then determined the effects of chronic thalamocortical inhibition on a different subcortical
241 projection, cortical cells from deep layers V/VI projecting to the MD thalamus. A rgGFP virus
242 was injected into the MD and whole cell patch clamp recordings were taken in thalamic
243 projecting cortical cells (Fig. 3a-b). Like for non-specific layer II/III and cortico-accumbens
244 neurons, we observed significant decreases in excitatory synaptic transmission (Fig. 3e-h).
245 Significant decreases were observed in both the frequency [$F(1, 6.73) = 12.960$, $p = 0.009$] and
246 spatial distribution (instantaneous frequency) [$F(1, 6.10) = 13.045$, $p = 0.011$] of sEPSCs but the
247 amplitude [$F(1, 5.36) = 0.689$, $p = 0.442$] of sEPSCs remained unchanged (Fig. 3e-f). In
248 addition, the frequency [$F(1, 6.39) = 7.829$, $p = 0.029$] and spatial distribution (instantaneous
249 frequency) [$F(1, 5.96) = 6.501$, $p = 0.044$] but not the amplitude [$F(1, 4.77) = 0.991$, $p = 0.367$]
250 of sIPSCs was reduced after P20-35 thalamic inhibition (Fig. 3g-h). These data show that like for
251 superficial layer II/III accumbens projections, adolescent thalamo-prefrontal inhibition also
252 decreases excitatory and inhibitory synaptic inputs to deep layer cortico-thalamic neurons.

253

254 **Adolescent thalamocortical activity regulates the amplitude of excitatory and**
255 **inhibitory currents in deep layer (V/VI) accumbens-projecting cortical cells.**

256 Accumbens projecting prefrontal neurons originate from both superficial and deep cortical layers
257 (Anastasiades and Carter, 2021). We therefore also recorded from accumbens-projecting cells in
258 layer V/VI. We found significant increases to excitatory and inhibitory current amplitude, and no
259 changes in frequency or spatial distribution, in deep layer accumbens-projecting cells (Fig 4e-h).
260 When measuring excitatory currents in deep layers, amplitude was significantly increased [$F(1,$
261 $29) = 8.976$, $p = 0.006$] however, frequency [$F(1, 5.49) = 7.841\text{x}10^{-5}$, $p = 0.993$] and spatial
262 distribution (instantaneous frequency) [$F(1, 6.24) = 0.196$, $p = 0.673$] remained unchanged (Fig
263 4e-f). Similar to excitatory transmission, for inhibitory currents in deeper layers, amplitude was
264 significantly increased [$F(1, 4.25) = 14.809$, $p = 0.013$] however, frequency [$F(1, 6.82) = 0.417$, p
265 $= 0.539$] and spatial distribution (instantaneous frequency) [$F(1, 6.53) = 0.910$, $p = 0.374$]
266 remained unchanged (Fig. 4 g-h). These data show that unlike layer II/III accumbens projection
267 neurons, excitatory and inhibitory drive onto layer V/VI accumbens neurons is not decreased and
268 not enhanced except at the level of amplitude.

269

270 **Adolescent thalamocortical activity regulates cross-hemispheric inhibition.**

271 To determine how adolescent thalamocortical inhibition impacts cortico-cortical circuitry, a rGFP
272 virus was injected into the dextral prelimbic mPFC and whole cell patch clamp recordings were
273 taken in cortically-projecting cortical cells in the sinistral hemisphere (Fig. 5a-b). No significant
274 differences were observed in the frequency [$F(1, 7.41) = 0.012$, $p = 0.917$], spatial distribution

275 (instantaneous frequency) [$F(1, 7.30) = 0.399$, $p = 0.547$] or amplitude [$F(1, 6.37) = 2.865$, $p =$
276 0.134] of excitatory events in cortical projecting cortical cells (Fig. 5e-f). Unlike excitatory
277 transmission, inhibitory transmission significantly increased in the distribution of events
278 (instantaneous frequency) [$F(1, 5.95) = 8.023$, $p = 0.030$] and trended in frequency [$F(1, 7.32) =$
279 4.185, $p = 0.078$] but not amplitude [$F(1, 62) = 0.112$, $p = 0.912$] after adolescent thalamocortical
280 inhibition (Fig. 5g-h). These findings were unexpected since callosal projecting prelimbic
281 neurons are enriched in layer II/III (Anastasiades et al., 2018) and the unspecific analysis of layer
282 II/III neurons displayed a decrease in the frequency of excitatory currents and no increase in
283 inhibition.
284

285 **Excitation-Inhibition balance is only altered in callosally projecting mPFC**
286 **neurons.**

287 Excitation and inhibition are well calibrated in prefrontal neurons (Yin et al., 2021) and in
288 agreement with this we found a strong correlation in the frequency of excitatory and inhibitory
289 currents for all control neurons across the cortex [R^2=0.4935, d.f. =1,121, P<0.0001] (Fig. 6a). In
290 many cell populations we observed changes in both excitation and inhibition, suggesting
291 homeostatic mechanisms may compensate for reduced excitatory drive from the thalamus. (Sup.
292 Fig. 1). We therefore calculated the excitation-inhibition balance in the different analyzed
293 populations of neurons. No changes in the excitation-inhibition balance were measured in layer
294 II/III and V/VI cortico-accumbens projecting neurons, and cortico-thalamic neurons (Fig. 6b-e).
295 In contrast, when analyzing the ratio of excitatory to inhibitory currents in callosally projecting
296 mPFC neurons, the frequency [$F(1, 11.37) = 5.697$, $p = 0.035$] and spatial distribution

297 (instantaneous frequency) [$F(1, 9.34) = 5.744$, $p = 0.039$] of excitatory to inhibitory currents was
298 significantly weighted towards inhibition (Fig. 6f).
299

300 **Discussion**

301 To determine the importance of thalamo-prefrontal activity for prefrontal circuit
302 maturation we inhibited thalamo-mPFC projections from P20-35 and recorded from prelimbic
303 neurons twenty-four hours later. We made several observations. First, our findings reveal that
304 excitatory transmission to layer II/III is already decreased during adolescence. This suggests that
305 the decrease in excitation measured in adult mice following this manipulation (Benoit et al.,
306 2022b) does not require full maturation of the circuitry to adulthood but arises early-on during
307 adolescence. Second, we measured decreased excitatory and inhibitory transmission to layer
308 II/III nucleus accumbens and layer V/VI thalamic-projecting neurons. These changes in
309 inhibition suggest that suppressing thalamic activity during adolescence leads to changes in
310 prefrontal connectivity beyond the loss of excitatory inputs from the thalamus that had
311 previously been observed at the anatomical level at P35 (Benoit et al., 2022b). Third, we
312 observed a surprising increase in excitatory and inhibitory transmission to layer V/VI NAc-
313 projecting neurons but at the level of sEPSC and sIPSC amplitude and not frequency. These
314 results suggest a post-synaptic adaptation in accumbens-projecting layer V/VI neurons. While
315 the reason for the specificity of this effect is unclear, cells projecting to the NAc located in deep
316 layers may have distinct molecular characteristics from those in superficial layers as molecular
317 characteristics differ between different layers (Bhattacherjee et al., 2019). Finally, we measured
318 an enhanced inhibition in cortico-cortical connectivity, which provides further evidence for a
319 complex prefrontal circuit adaptation in response to thalamic inhibition. Intriguingly, while

320 excitatory and inhibitory drive was altered onto subcortically projection neurons, a change in the
321 balance of excitation and inhibition was only measured in cross-hemispheric mPFC projections
322 and not in the three subcortical projections analyzed. As functional stability in neural circuits can
323 be sustained by homeostatic re-balancing of excitatory and inhibitory inputs, the largest
324 functional effect of adolescent thalamocortical inhibition on prefrontal circuitry may be a
325 decrease in the activity of contralaterally-projecting mPFC pyramidal cells. While it is difficult
326 to predict neuronal activity in vivo from slice physiological measures, enhanced inhibitory inputs
327 to cross-hemispheric projection neurons may lead to less activity of these neurons during
328 adolescence, which may have long lasting consequences for mPFC network function in the adult.
329 Future studies will be able to address whether disinhibition of cross hemispheric projections
330 during adolescence following thalamocortical inhibition will rescue the long-term negative
331 effects of the earlier thalamocortical inhibition.
332

333 **Decreased excitatory transmission in superficial mPFC arises during**
334 **adolescence.**

335 Previous work from our group demonstrated that adolescent thalamic inhibition during a
336 critical period (P20-P50) resulted in long term cognitive and physiological deficits in the
337 adult mouse, including a loss of excitatory transmission in non-projection-specific layer
338 II/III pyramidal cells. Here, we observe these deficits are already established during
339 adolescence, prior to being sustained into adulthood. This dampening of excitatory
340 transmission onto layer II/III neurons could result from the loss of primary MD innervation
341 to excitatory pyramidal cells or a loss of local excitation through local feed forward
342 excitation or both. The seemingly bimodal distribution of the effects in layer II/III neurons

343 led us to hypothesize that thalamocortical inhibition may be differentially affecting
344 subpopulations of neurons in layer II/III of the mPFC. To distinguish these effects on
345 distinct populations of cortical cells, we focused our first analysis on NAc projecting mPFC
346 neurons.
347
348 **Adolescent thalamocortical activity regulates excitatory and inhibitory transmission to**
349 **superficial nucleus accumbens projecting pyramidal cells.**
350 Excitatory and inhibitory currents were both decreased in NAc-projecting cortical cells
351 following adolescent thalamic inhibition. These data provide evidence that altering
352 thalamic input activity during adolescence may have widespread effects on cells projecting
353 to a variety of regions, including mPFC-NAc projections that are essential for reward driven
354 motivated behaviors (Kalivas et al., 2005; Mannella et al., 2013; McGlinchey et al., 2016)
355 Adolescent inhibited mice may therefore not only have deficits in attentional set shifting
356 and working memory task but also more broadly in reward-driven motivated behaviors.
357
358 The decrease in the frequency of inhibitory events could be the consequence of a reduction
359 in thalamic projections onto interneurons (Yang et al., 2021). For example, the MD directly
360 innervates layer II/III parvalbumin (PV+) and other interneurons, providing a source of
361 feedforward inhibition to cortical projection neurons (Delevich et al., 2015; Canetta et al., 2020).
362 Changes in interneuron-driven inhibition in NAc projecting cells measured in the slice could
363 reflect either reduced excitatory drive on PV+ cells, or anatomical and functional adaptations
364 within PV+ interneurons following thalamic inhibition. Future studies directly measuring
365 excitatory and inhibitory currents in PV+ cells or other cortical interneurons as well as using

366 optogenetic approaches to probe functional connectivity between those specific interneurons and
367 NAc-projecting neurons will be able to address this.
368 Moreover, the decrease in inhibitory transmission within this cell population is distinct from
369 other populations in the prelimbic cortex, namely layer II/III cortico-cortical cells, which show
370 increased levels of inhibition following adolescent thalamic inhibition. These findings
371 underscore the complex effects on excitatory and inhibitory connectivity elicited by adolescent
372 thalamocortical inhibition in layer II/III pyramidal cells in the prefrontal cortex. To determine
373 whether adolescent thalamic inhibition also alters excitatory and inhibitory connections in deeper
374 layers of the mPFC, we next recorded from cortico-thalamic neurons in layer V/VI.
375
376 **Adolescent thalamic inhibition decreases excitatory and inhibitory drive to prefrontal**
377 **projections to the thalamus, further dysregulating the MD-mPFC circuit.**
378 We found that adolescent thalamic inhibition resulted in a decrease in the frequency of
379 excitatory and inhibitory currents in thalamus projecting cells in layer V/VI, of the mPFC,
380 similar to the effects seen in NAc-projecting cells in layer II/III. The MD primarily projects
381 to layer II/III; however, slice physiology has demonstrated monosynaptic connection to the
382 deeper layers (V/VI) of the cortex, including direct reciprocal connection (Collins et al.,
383 2018). The origins for the decrease in excitatory and inhibitory drive may therefore be
384 similar to ones measured in layers II/III.
385
386 **Deeper (V/VI) accumbens projecting cortical cells show post-synaptic adaptation to**
387 **MD inhibition.**

388 Surprisingly, we found that following adolescent thalamic inhibition the amplitude of
389 excitatory and inhibitory currents increased in layer V/VI accumbens projecting neurons**,**
390 while the frequency and spatial distribution remained the same. While the thalamus makes
391 direct connections onto deep layer pyramidal cells (Collins et al., 2018) it is unknown
392 whether the MD directly innervates layer V/VI NAc projecting cells. One possibility is that
393 sEPSC frequency is unaffected in this cell population because it does not receive much
394 direct thalamic input. Adolescent thalamic inhibition further increased sEPSC amplitude in
395 these cells. As changes in amplitude are thought to reflect post-synaptic alterations, this
396 increase in the sEPSC amplitude may be a post-synaptic adaptation though it is currently
397 unclear what exactly the increased amplitude is compensating for. This increase in sEPSC
398 amplitude further emphasizes the diverse adaptive and complex changes that thalamocortical
399 inhibition can produce.

400

401 **Callosally projecting cells display an increase in inhibitory inputs following adolescent**
402 **thalamic inhibition.**

403 The frequency of excitatory inputs to contralaterally projecting mPFC neurons did not
404 change following adolescent thalamic inhibition. However, inhibitory inputs were increased.
405 The absence of an effect of adolescent thalamic inhibition on excitatory current frequency in
406 this population is surprising, given that they receive some of the strongest direct inputs from
407 the MD (Anastasiades et al., 2018). Why excitatory inputs to this population are spared
408 remains unknown, but it suggests that excitatory inputs from other brain regions may be
409 able to offset the reduction in excitatory inputs from the thalamus. This hypothesis could be
410 directly addressed in future studies using optogenetics to probe the strength of functional

411 connections made by distinct excitatory connections onto callosally projecting cells. The
412 increase in inhibition observed in this population is also surprising, given that inhibition was
413 decreased in NAc projecting cells found in the same cortical layer. Moreover, while changes
414 in excitation and inhibition driven by adolescent thalamic inhibition largely scaled in all
415 other cell populations analyzed, cortico-cortical projecting cells showed a significant
416 reduction in their E/I sPSC ratio.
417 Overall, the relative stability of the E/I sPSC ratio following adolescent thalamic inhibition
418 is consistent with the idea of a homeostatic regulation in subcortically projecting neurons
419 such that the decrease in inhibition may be an adaptive consequence to the decrease in
420 excitatory inputs they receive from the thalamus. However, in cortically projecting neurons,
421 thalamic inhibition resulted in an increase in inhibition with no effect on excitation, and a
422 significant reduction in E/I balance in these cells. One prediction of this finding would be
423 that cortically projecting neurons might experience the greatest overall change in their
424 activation profile following adolescent thalamic inhibition, with the net effect of being less
425 active in vivo. This change may in turn contribute to a lack of cross-hemispheric cortical
426 communication, and bilateral recruitment of the prefrontal cortex has been hypothesized to
427 be important for cognitive processes (Hasegawa et al., 1998; Holler-Wallscheid et al., 2017).
428 This change may also decrease cortical output to other neural circuits, including the nucleus
429 accumbens and mediodorsal thalamus, thereby having widespread effects on prefrontal
430 network function.
431 Alternatively, the increase in contralateral inhibition following adolescent thalamocortical
432 silencing may have resulted from disinhibition via either the release of inhibition on
433 somatostatin positive interneurons (SST+) by vasoactive intestinal polypeptide (VIP+)

interneurons or release of inhibition on PV+ interneurons by somatostatin positive interneurons. VIP+ interneurons receive direct MD input and have strong connections with SST+ neurons (Ahrlund-Richter et al., 2019; Sun et al., 2019; Canetta et al., 2020). SST+ neurons project onto PV+ cells and the apical dendrites of pyramidal cells. Like PV+ and VIP+ interneurons, SST+ interneurons are also known to receive direct inputs from the MD (Ahrlund-Richter et al., 2019; Sun et al., 2019). Therefore, the overall increase in inhibition could be due to the complex disinhibitory circuit between VIP+, SOM+, PV+ and pyramidal cell types. It is unclear why this disinhibition should be specific only to cross hemispheric, intracortical connectivity. While no studies have directly addressed this question, PV interneurons target callosally projecting pyramidal cells (Cho et al., 2023) while VIP+ and SST+ neurons preferentially target other interneuron populations in the cortex (Pi et al., 2013). Given the specific increase in the density of inhibitory transmission, this could be the result of decreased inhibition of PV+ interneurons by SST+ or VIP+ interneurons causing an increase in the inhibition of callosal projections.

Possible mechanisms of mPFC plasticity induced by adolescent thalamic inhibition.

Recent studies also point to intra-cortical mechanisms in the maturation of cortical circuitry. Anterior cingulate (ACC) neurons show greater excitatory synaptic inputs during adolescence than adulthood and DREADD-mediated inhibition of ACC to visual cortex projection neurons during adolescence has been shown to disrupt the maintenance of local connectivity within the ACC (Nabel and Morishita, 2013). We also measured an increase in the frequency of excitatory currents in adolescent mice (5.631+/- 0.466) when compared to adult mice in Benoit et al. 2022 (4.4+-0.4 Hz). By analogy, if inhibition of thalamic inputs decreases activity of mPFC-thalamic

457 or accumbens projection neurons during adolescence, this may lead to a disruption in the
458 maintenance of local excitation in the mPFC. A different mechanism has also been described
459 within the visual cortex. DREADD-mediated inhibition of layer II/III neurons during the critical
460 period of primary visual cortex development (P24-29) (Wen and Turrigiano, 2021) (Nabel et al.,
461 2020) led to excitatory synaptic scaling and increased intrinsic excitability suggesting
462 homeostatic plasticity as a mechanism affecting visual cortex maturation. Future studies will be
463 able to identify the exact plasticity mechanisms in mPFC circuitry that are induced by thalamic
464 inhibition during adolescence.
465
466 **How these findings will scale to the adult mouse remain unknown.**
467 Finally, how do the changes observed in adolescence (P35) relate to physiology and behavior in
468 the adult mouse? While we have observed similar effects on sEPSC frequency in non-specific
469 layer II/III cells at both P35 and in adulthood, it will be of interest to see whether the other
470 changes we have identified also scale into adulthood. If they did, this would be consistent with
471 the idea that P20-35 is an activity dependent sensitive period in which manipulating the activity
472 of thalamic inputs to the mPFC leads to changes in the wiring of that circuitry that are then
473 'hardwired' until adulthood.
474 Alternatively, changes identified in adolescence may represent a transient change in circuit
475 dynamics, that then sets in motion subsequent and different changes in circuit dynamics that
476 result in altered prefrontal network function in adulthood. In this scenario, changes in synaptic
477 connectivity in adolescent inhibited mice may be different immediately after the inhibition than
478 later during adulthood, a hypothesis that could be addressed by further recordings in adult
479 animals.

480 **Conclusions:**

481 In sum, our data demonstrate thalamic inhibition during a sensitive period in adolescence results
482 in projection specific changes in synaptic connectivity in the mPFC that become evident already
483 during adolescence. The dysregulation of multiple neural circuits demonstrates the widespread
484 effects of thalamo-prefrontal inhibition that impact more than just thalamocortical circuitry.
485 Further, the observed deficits cannot be explained just by a lack of anatomical input. Rather, they
486 generate widespread adaptative or possibly maladaptive physiological responses within
487 prefrontal circuitry. Future studies will examine which of these projection specific changes
488 persist into adulthood, whether new ones emerge and whether they represent appropriate targets
489 for intervention during adolescence.

Figure 1

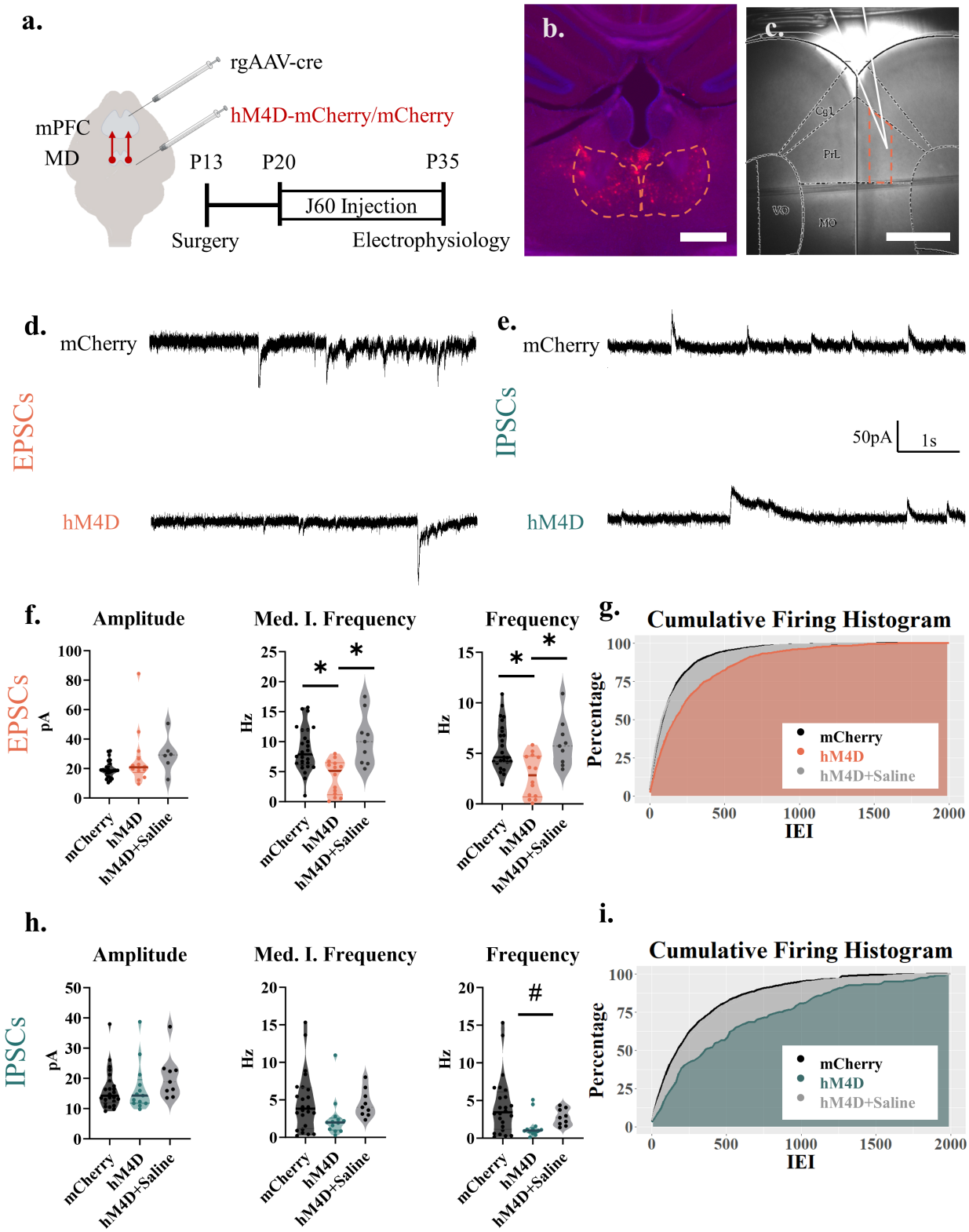
a.
rgAAV-cre
hM4D-mCherry/mCherry
mPFC
MD
P13
P20
P35
J60 Injection
Surgery
Electrophysiology
b.
c.
CgL
PrL
VO
MO
d.
mCherry
EPSCs
hM4D
e.
mCherry
IPSCs
50pA
1s
hM4D
f.
Amplitude
Med. I. Frequency
Frequency
EPSCs
pA
Hz
mCherry
hM4D
hM4D+Saline
g.
Cumulative Firing Histogram
Percentage
IEI
mCherry
hM4D
hM4D+Saline
h.
Amplitude
Med. I. Frequency
Frequency
IPSCs
pA
Hz
mCherry
hM4D
hM4D+Saline
i.
Cumulative Firing Histogram
Percentage
IEI
mCherry
hM4D
hM4D+Saline

Figure 1) **Adolescent thalamocortical activity regulates excitatory transmission to superficial mPFC**. **a**, Adolescent experimental timeline, and schematic. Whole-cell patch clamp recordings were made from pyramidal cells in layer II/III of the mPFC from hM4D and control mice. These pyramidal cells receive excitatory inputs from the thalamus as well as inhibitory inputs from local interneurons; created with https://biorender.com. **b**, Example image illustrating hM4D-mCherry expression in the mediodorsal thalamus (orange outline) in adolescent animals. Histology images were collected from each animal for each cohort, with at least 6 slices taken for each animal. Scale bar represents 300µm. **c**, Example image illustrating the recording location in the prelimbic (PrL) subregion of the medial prefrontal cortex. All recordings for this experiment were conducted in this region approximately 200-350µm from the pial surface (L II/III) denoted by the orange dotted line. Recording pipette outlined in white. Scale bar represents 500µm **d**, Representative traces showing sEPSCs of hM4D animals and mCherry controls. **e**, Representative traces showing sIPSCs of hM4D animals and mCherry controls. **f**, sEPSC frequency (right) and median instantaneous frequency (middle) is significantly reduced following adolescent thalamic inhibition relative to control mice, but sEPSC amplitude (left) is unchanged; mCherry control, $n = 26$ cells and 6 animals; hM4D, $n = 14$ cells and 5 animals; hM4D+Saline n=9 cells and 2 animals; frequency: mCherry control 4.617(3.050) Hz, hM4D 2.833(3.858) Hz, and hM4D+Saline 5.733(2.700) Hz, contrasts of estimated marginal means revealed a significant difference between hM4D animals and both mCherry, $z = -3.311.129$, d.f. = ∞ *$P_{bonferroni} = 0.003$, and hM4D+Saline, $z = 3.035$, d.f. = ∞ *$P_{bonferroni} = 0.007$ but no significant difference between mCherry and hM4D+Saline, $z = 0.501$, d.f. = ∞ *$P_{bonferroni} = 1.000$; median instantaneous frequency: mCherry control 7.892(5.340) Hz, hM4D 5.126(4.882) Hz, hM4D+Saline 10.005(4.989) Hz; contrasts of estimated marginal means revealed a significant difference between hM4D animals and both mCherry, $z = -3.032$, d.f. = ∞ *$P_{bonferroni} = 0.007$, and hM4D+Saline, $z = 3.348$, d.f. = ∞ *$P_{bonferroni} = 0.002$ but no significant difference between mCherry and hM4D+Saline, $z = 1.097$, d.f. = ∞ *$P_{bonferroni} = 0.818$; amplitude: mCherry control 18.785(5.250) pA, hM4D 20.916(4.882) pA, and hM4D+Saline 28.786(5.782) pA. All reported values are Median(Interquartile Range). **g**, Graph of the cumulative firing distribution for sEPSCs in L 2/3 pyramidal cells in the mPFC, IEI represents the interevent-interval between spontaneous events. **h**, sIPSC frequency (right) may trend downwards but median instantaneous frequency (middle) and amplitude (left) are unchanged following adolescent thalamic inhibition relative to control mice; mCherry control, $n = 26$ cells and 6 animals; hM4D, $n = 14$ cells and 5 animals; frequency: mCherry control 2.500(3.267) Hz, hM4D 1.000(0.550) Hz and hM4D+Saline 2.717(1.833); median instantaneous frequency: mCherry control 3.826(5.039) Hz, hM4D 1.989(1.256) Hz, and hM4D+Saline 4.014(2.366; amplitude: mCherry control 14.264(5.638) pA, hM4D 14.3(6.075) pA, and hM4D+Saline 18.849(6.737). All reported values are Median(Interquartile Range). **i**, Graph of the cumulative firing distribution for sIPSCs in L 2/3 pyramidal cells in the mPFC, IEI represents the interevent-interval between spontaneous events. *P<0.05, #P~0.10.

Figure 2

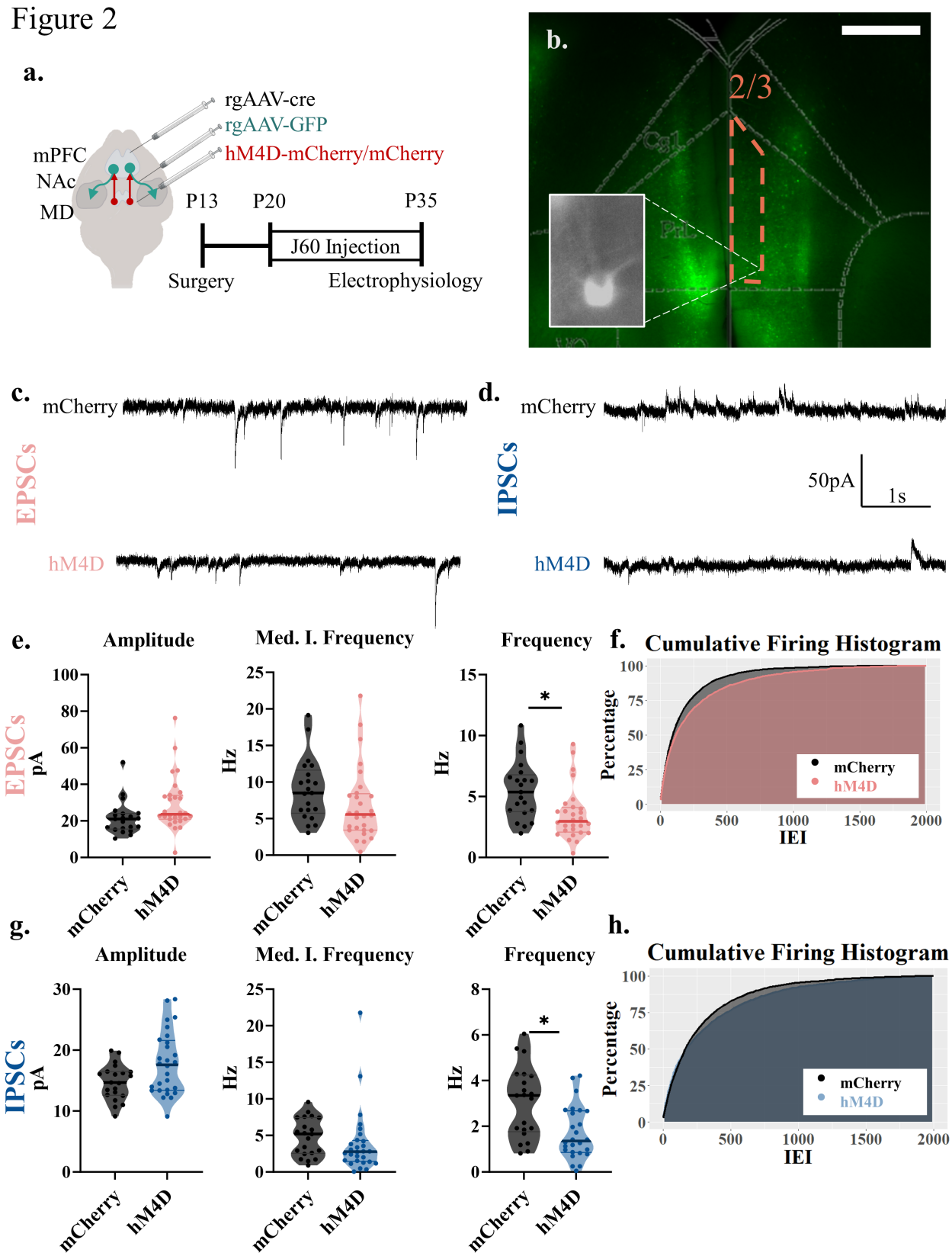
a.
rgAAV-cre
rgAAV-GFP
hM4D-mCherry/mCherry
mPFC
NAc
MD
P13
P20
P35
J60 Injection
Surgery
Electrophysiology
b.
2/3
c.
mCherry
EPSCs
hM4D
d.
mCherry
IPSCs
50pA
1s
hM4D
e.
Amplitude
Med. I. Frequency
Frequency
EPSCs
pA
Hz
mCherry
hM4D
f.
Cumulative Firing Histogram
Percentage
IEI
mCherry
hM4D
g.
Amplitude
Med. I. Frequency
Frequency
IPSCs
pA
Hz
mCherry
hM4D
h.
Cumulative Firing Histogram
Percentage
IEI
mCherry
hM4D

Figure 2) Adolescent thalamocortical activity regulates excitatory and inhibitory transmission to superficial layer II/III cortico-accumbens projections. a, Adolescent experimental timeline and schematic. Whole-cell patch clamp recordings were made from accumbens projecting pyramidal cells in layer II/III of the mPFC from hM4D and control mice; Created with https://biorender.com. **b**, Example image illustrating rGFP positive, accumbens projecting cells in the prelimbic subregion of the medial prefrontal cortex. Scale bar represents 500µm. **c**, Representative traces showing sEPSCs of hM4D animals and mCherry controls. **d**, Representative traces showing sIPSCs of hM4D animals and mCherry controls**. e**, sEPSC frequency (right) is significantly reduced in accumbens projecting cortical cells following adolescent thalamic inhibition relative to control mice, but sEPSC amplitude (left) and median instantaneous frequency (middle) are unchanged; mCherry control, $n = 21$ cells and 5 animals; hM4D, $n = 28$ cells and 6 animals; frequency: mCherry control 5.367(2.717) Hz, hM4D 2.975(1.871) Hz.; median instantaneous frequency: mCherry control 8.514(4.842) Hz and hM4D 5.579(4.803) Hz; amplitude: mCherry control 21.051(7.992) pA and hM4D 23.648(12.495) pA. All reported values are Median(Interquartile Range). **f**, Graph of the cumulative firing distribution for sEPSCs in L II/III accumbens projecting pyramidal cells in the mPFC, IEI represents the interevent-interval between spontaneous events. **g**, sIPSC frequency (right) is significantly reduced in accumbens projecting cortical cells following adolescent thalamic inhibition relative to control mice, but sIPSC amplitude (left) and median instantaneous frequency (middle) are unchanged; mCherry control, $n = 21$ cells and 5 animals; hM4D, $n = 28$ cells and 6 animals; frequency: mCherry control 3.350(2.350) Hz, hM4D 1.417(1.762) Hz; median instantaneous frequency: mCherry control 5.195(4.817) Hz and hM4D 2.776(2.753) Hz; amplitude: mCherry control 14.618(3.768) pA and hM4D 17.597(7.919) pA. All reported values are Median(Interquartile Range). **h**, Graph of the cumulative firing distribution for sIPSCs in L II/III accumbens projecting pyramidal cells in the mPFC. *$P<0.05$.

490

Figure 3

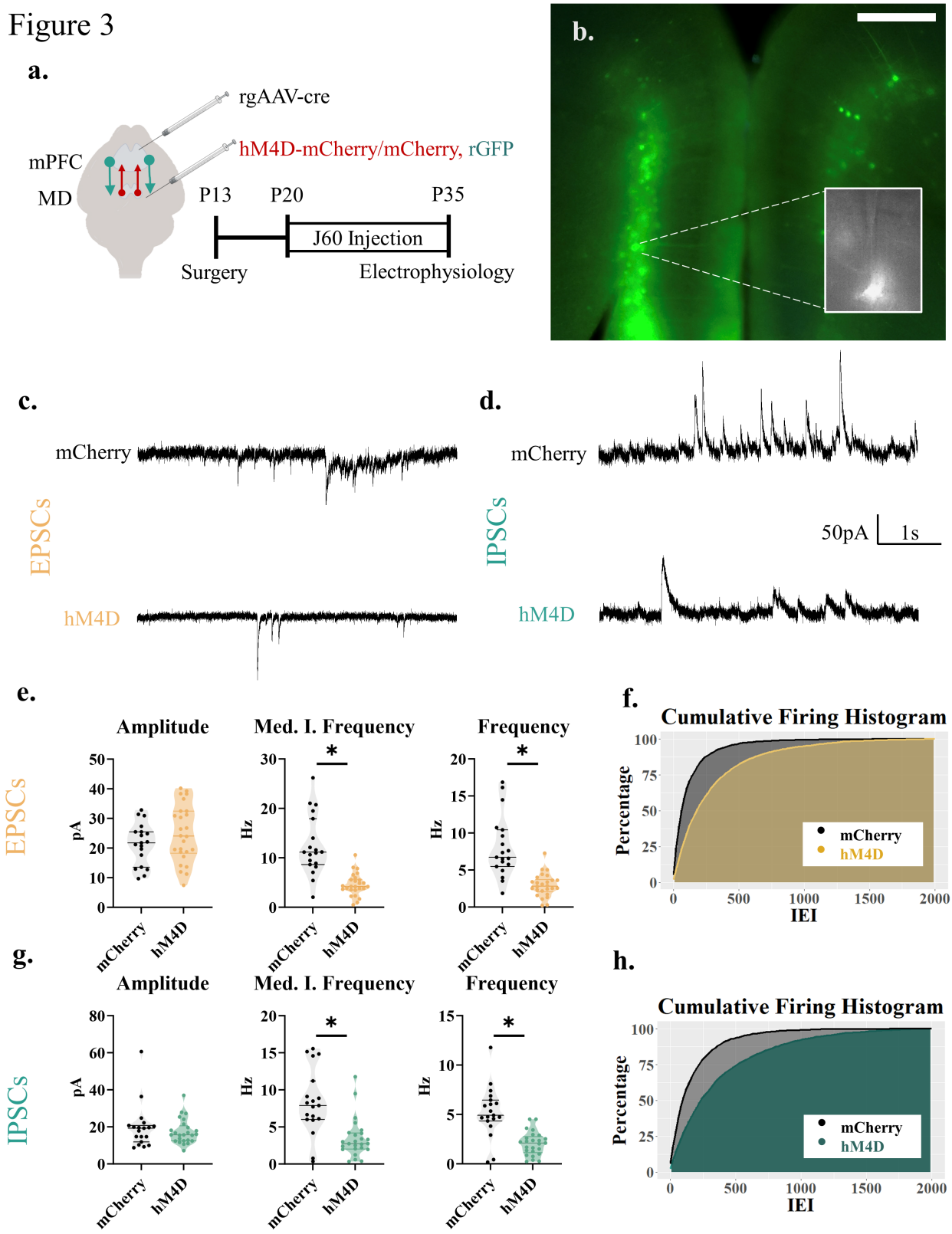
a.
rgAAV-cre
hM4D-mCherry/mCherry, rGFP
mPFC
MD
P13
P20
P35
J60 Injection
Surgery
Electrophysiology
b.
c.
mCherry
EPSCs
hM4D
d.
mCherry
IPSCs
50pA
1s
hM4D
e.
EPSCs
Amplitude
Med. I. Frequency
Frequency
pA
Hz
mCherry
hM4D
f.
Cumulative Firing Histogram
Percentage
IEI
mCherry
hM4D
g.
IPSCs
Amplitude
Med. I. Frequency
Frequency
h.
Cumulative Firing Histogram
Percentage
IEI
mCherry
hM4D

Figure 3) Adolescent thalamocortical activity regulates excitatory and inhibitory transmission to cortico-thalamic projections. a, Adolescent experimental timeline, and schematic. Whole-cell patch clamp recordings were made from cortical projecting pyramidal cells in layer V/VI of the mPFC from hM4D and control mice. These pyramidal cells receive excitatory inputs from the thalamus and superficial layers of the cortex as well as inhibitory inputs from local interneurons; created with https://biorender.com. **b**, Example image illustrating rGFP positive cells in the prelimbic subregion of the medial prefrontal cortex. All recordings for this experiment were conduced in this region approximately 500-600µm from the pial surface (L V/VI). Scale bar represents 300µm **c**, Representative traces showing sEPSCs of hM4D animals and mCherry controls. **d**, Representative traces showing sIPSCs of hM4D animals and mCherry controls**. e**, sEPSC frequency (right) and median instantaneous frequency (middle) is significantly reduced in thalamic projecting cortical cells following adolescent thalamic inhibition relative to control mice, but sEPSC amplitude (left) is unchanged; mCherry control, $n = 19$ cells and 4 animals; hM4D, $n = 26$ cells and 5 animals; frequency: mCherry control 6.717(4.392) Hz and hM4D 2.833(1.408) Hz; median instantaneous frequency: mCherry control 11.173(7.187) Hz and hM4D 4.204(1.997) Hz; amplitude: mCherry control 21.764(9.897) pA and hM4D 24.043(13.508) pA. All reported values are Median(Interquartile Range). **f**, Graph of the cumulative firing distribution for sEPSCs in L V/VI thalamic projecting pyramidal cells in the mPFC, IEI represents the interevent-interval between spontaneous events. **g**, sIPSC frequency (right) and median instantaneous frequency (middle) is significantly reduced in thalamic projecting cortical cells following adolescent thalamic inhibition relative to control mice, but sIPSC amplitude (left) is unchanged; mCherry control, $n = 19$ cells and 4 animals; hM4D, $n = 26$ cells and 5 animals; frequency: mCherry control 4.917(1.825) Hz and hM4D 2.100(1.350) Hz; median instantaneous frequency: mCherry control 7.896(4.100) Hz and hM4D 2.755(2.081) Hz; amplitude: mCherry control 19.267(7.264) pA and hM4D 15.720(7.127) pA. All reported values are Median(Interquartile Range). **h**, Graph of the cumulative firing distribution for sIPSCs in L V/VI thalamic projecting pyramidal cells in the mPFC. *$P<0.05$.

Figure 4

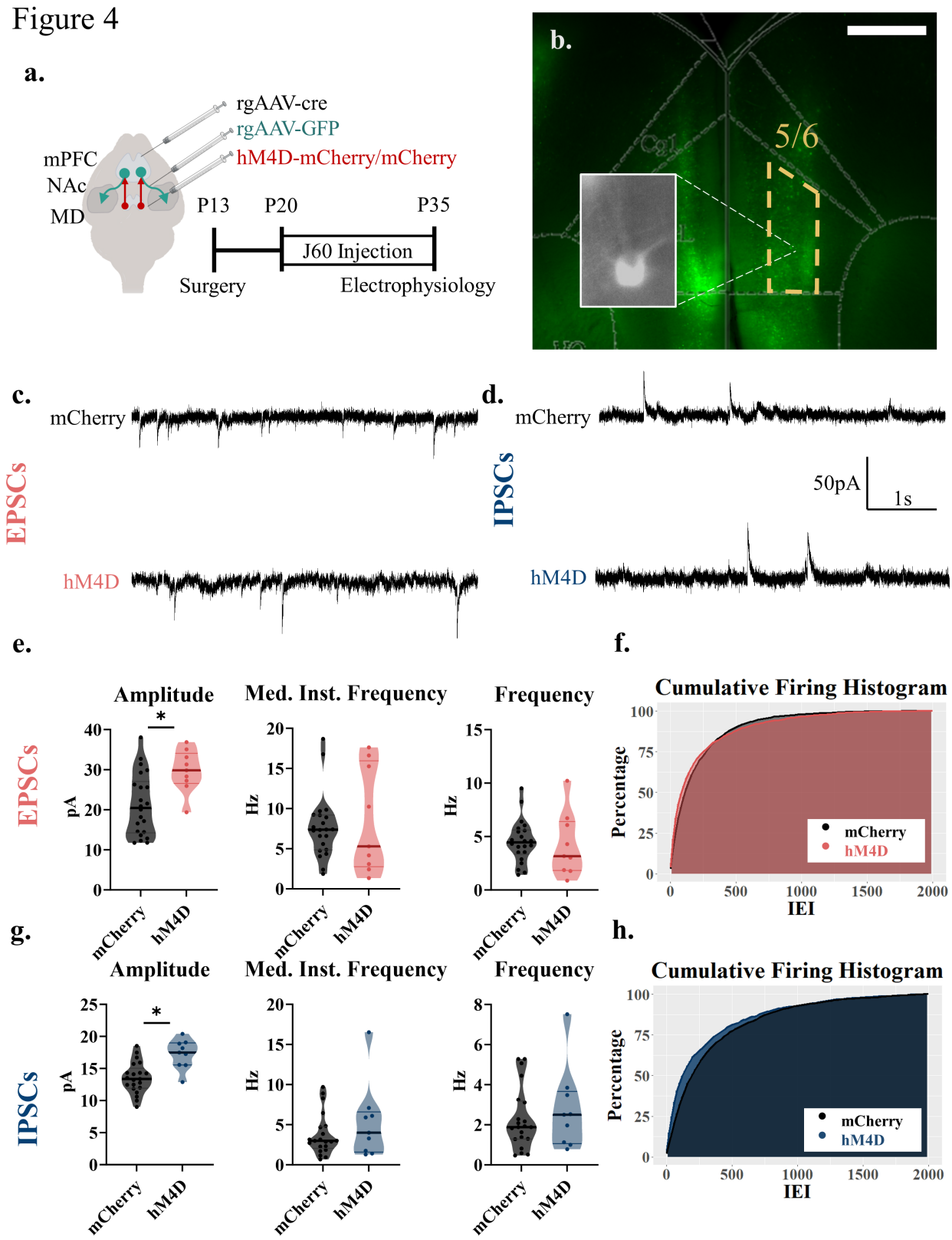
a.
rgAAV-cre
rgAAV-GFP
hM4D-mCherry/mCherry
mPFC
NAc
MD
P13
P20
P35
J60 Injection
Surgery
Electrophysiology
b.
5/6
c.
mCherry
EPSCs
hM4D
d.
mCherry
IPSCs
50pA
1s
hM4D
e.
Amplitude
Med. Inst. Frequency
Frequency
EPSCs
pA
Hz
mCherry
hM4D
f.
Cumulative Firing Histogram
Percentage
IEI
mCherry
hM4D
g.
Amplitude
Med. Inst. Frequency
Frequency
IPSCs
pA
Hz
mCherry
hM4D
h.
Cumulative Firing Histogram
Percentage
IEI
mCherry
hM4D

Figure 4) Adolescent thalamocortical activity results in enhanced amplitude in deeper (V/VI) accumbens projecting cortical cells. a, Adolescent experimental timeline and schematic. Whole-cell patch clamp recordings were made from accumbens projecting pyramidal cells in layer V/VI of the mPFC from hM4D and control mice; Created with https://biorender.com. **b**, Example image illustrating rGFP positive, accumbens projecting cells in the prelimbic subregion of the medial prefrontal cortex. Scale bar represents 500µm. **c**, Representative traces showing sEPSCs of hM4D animals and mCherry controls. **d**, Representative traces showing sIPSCs of hM4D animals and mCherry controls**. e**, sEPSC amplitude (left) is significantly increased in accumbens projecting cortical cells following adolescent thalamic inhibition relative to control mice, but sEPSC frequency (right) and median instantaneous frequency (middle) are unchanged; mCherry control, $n = 22$ cells and 5 animals; hM4D, $n = 9$ cells and 4 animals; frequency: mCherry control 4.450(2.012) Hz, hM4D 3.167(4.217) Hz.; median instantaneous frequency: mCherry control 7.371(4.043) Hz and hM4D 5.290(12.190) Hz; amplitude: mCherry control 20.460(11.638) pA and hM4D 29.858(5.869). All reported values are Median(Interquartile Range). **f**, Graph of the cumulative firing distribution for sEPSCs in L II/III accumbens projecting pyramidal cells in the mPFC, IEI represents the interevent-interval between spontaneous events. **g**, sIPSC frequency (right) is significantly reduced in accumbens projecting cortical cells following adolescent thalamic inhibition relative to control mice, but sIPSC amplitude (left) and median instantaneous frequency (middle) are unchanged; mCherry control, $n = 21$ cells and 5 animals; hM4D, $n = 28$ cells and 6 animals; frequency: mCherry control 1.883(1.817) Hz, hM4D 2.50(2.350) Hz; median instantaneous frequency: mCherry control 2.997(2.405) Hz and hM4D 4.005(4.349) Hz; amplitude: mCherry control 13.362(2.306) pA and hM4D 17.495(3.331). All reported values are Median(Interquartile Range). **h**, Graph of the cumulative firing distribution for sIPSCs in L V/VI accumbens projecting pyramidal cells in the mPFC. *P<0.05.

491

Figure 5

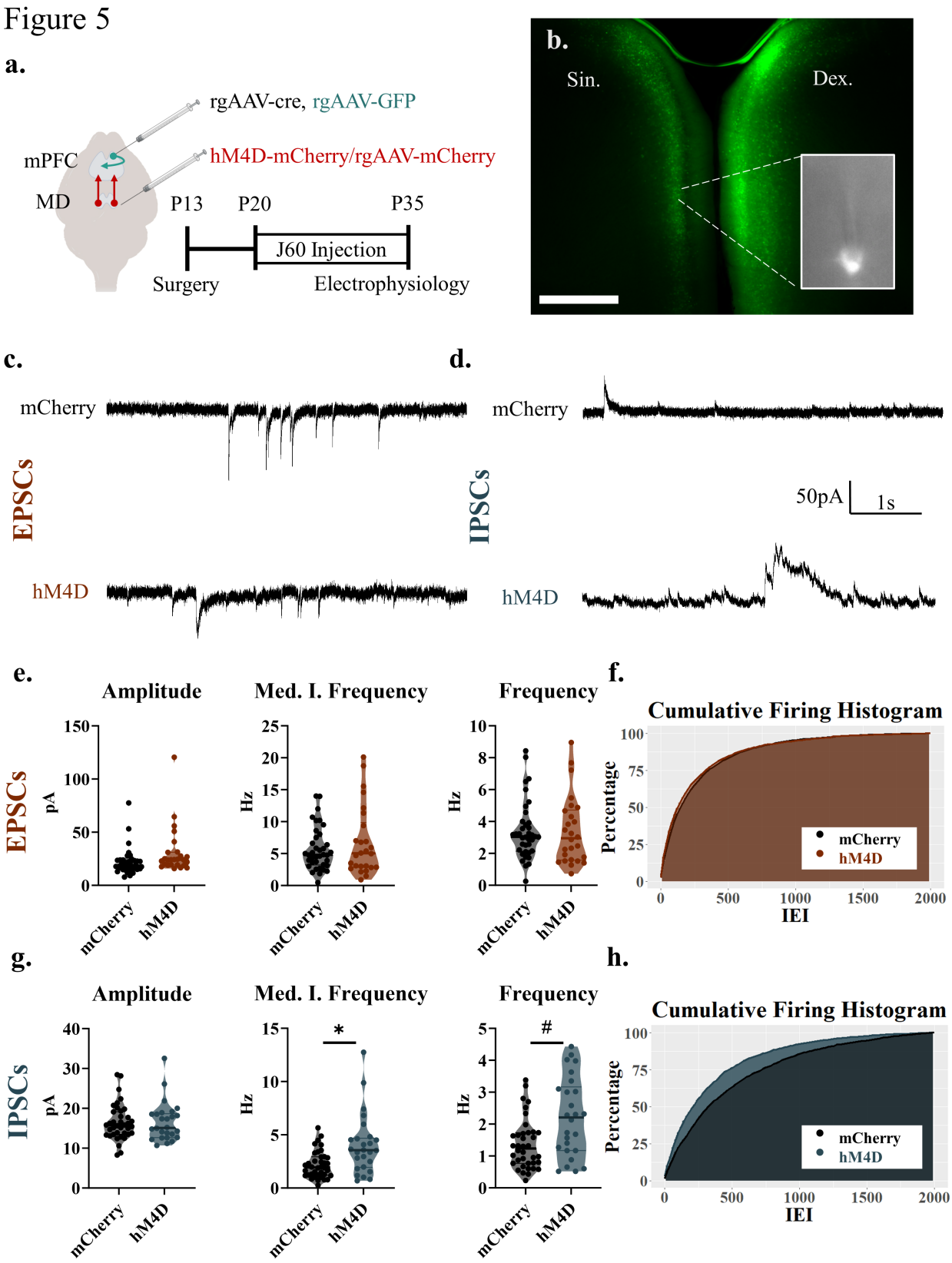
a.
rgAAV-cre, rgAAV-GFP
hM4D-mCherry/rgAAV-mCherry
mPFC
MD
P13
P20
P35
J60 Injection
Surgery
Electrophysiology
b.
Sin.
Dex.
c.
mCherry
EPSCs
hM4D
d.
mCherry
IPSCs
50pA
1s
hM4D
e.
Amplitude
Med. I. Frequency
Frequency
EPSCs
pA
Hz
mCherry
hM4D
f.
Cumulative Firing Histogram
Percentage
IEI
mCherry
hM4D
g.
Amplitude
Med. I. Frequency
Frequency
IPSCs
pA
Hz
*
#
mCherry
hM4D
h.
Cumulative Firing Histogram
Percentage
IEI
mCherry
hM4D

Figure 5) Adolescent thalamocortical activity regulates cross-hemispheric inhibition. a, Adolescent experimental timeline and schematic. Whole-cell patch clamp recordings were made from cortical projecting pyramidal cells in layer II/III of the mPFC from hM4D and control mice; Created with https://biorender.com. **b**, Example image illustrating rGFP positive, cortical projecting cells in the prelimbic subregion of the medial prefrontal cortex. Virus was injected into the dextral (right) hemisphere and cells were recorded only in the sinistral (left) hemisphere. Scale bar represents 500µm. **c**, Representative traces showing sEPSCs of hM4D animals and mCherry controls. **d**, Representative traces showing sIPSCs of hM4D animals and mCherry controls**. e**, sEPSC frequency (right), sEPSC amplitude (left) and sEPSC median instantaneous frequency are unchanged in cortical projecting cortical cells following adolescent thalamic inhibition relative to control mice; mCherry control, $n = 38$ cells and 5 animals; hM4D, $n = 26$ cells and 5 animals; frequency: mCherry control 3.042(1.713) Hz and hM4D 2.95(2.933) Hz; median instantaneous frequency: mCherry control 4.807(3.944) Hz and hM4D 5.042(5.890) Hz; amplitude: mCherry control 17.876(7.549) pA and hM4D 23.951(8.397) pA. All reported values are Median(Interquartile Range). **f**, Graph of the cumulative firing distribution for sEPSCs in cortical projecting pyramidal cells in the mPFC, IEI represents the interevent-interval between spontaneous events. **g**, sIPSC median instantaneous frequency (middle) is significantly increased and frequency (right) is trending towards an increase in cortical projecting cortical cells following adolescent thalamic inhibition relative to control mice, while amplitude (left) is unchanged; mCherry control, $n = 38$ cells and 5 animals; hM4D, $n = 26$ cells and 5 animals; frequency: mCherry control 1.233(0.954) Hz and hM4D 2.208(1.887) Hz; median instantaneous frequency: mCherry control 1.937(1.676) Hz and hM4D 5.551(2.498); amplitude: mCherry control 15.735(5.268) pA and hM4D 15.099(5.667) pA. All reported values are Median(Interquartile Range). **h**, Graph of the cumulative firing distribution for sIPSCs in cortical projecting pyramidal cells in the mPFC. *$P<0.05$, #$P<0.10$.

Figure 6

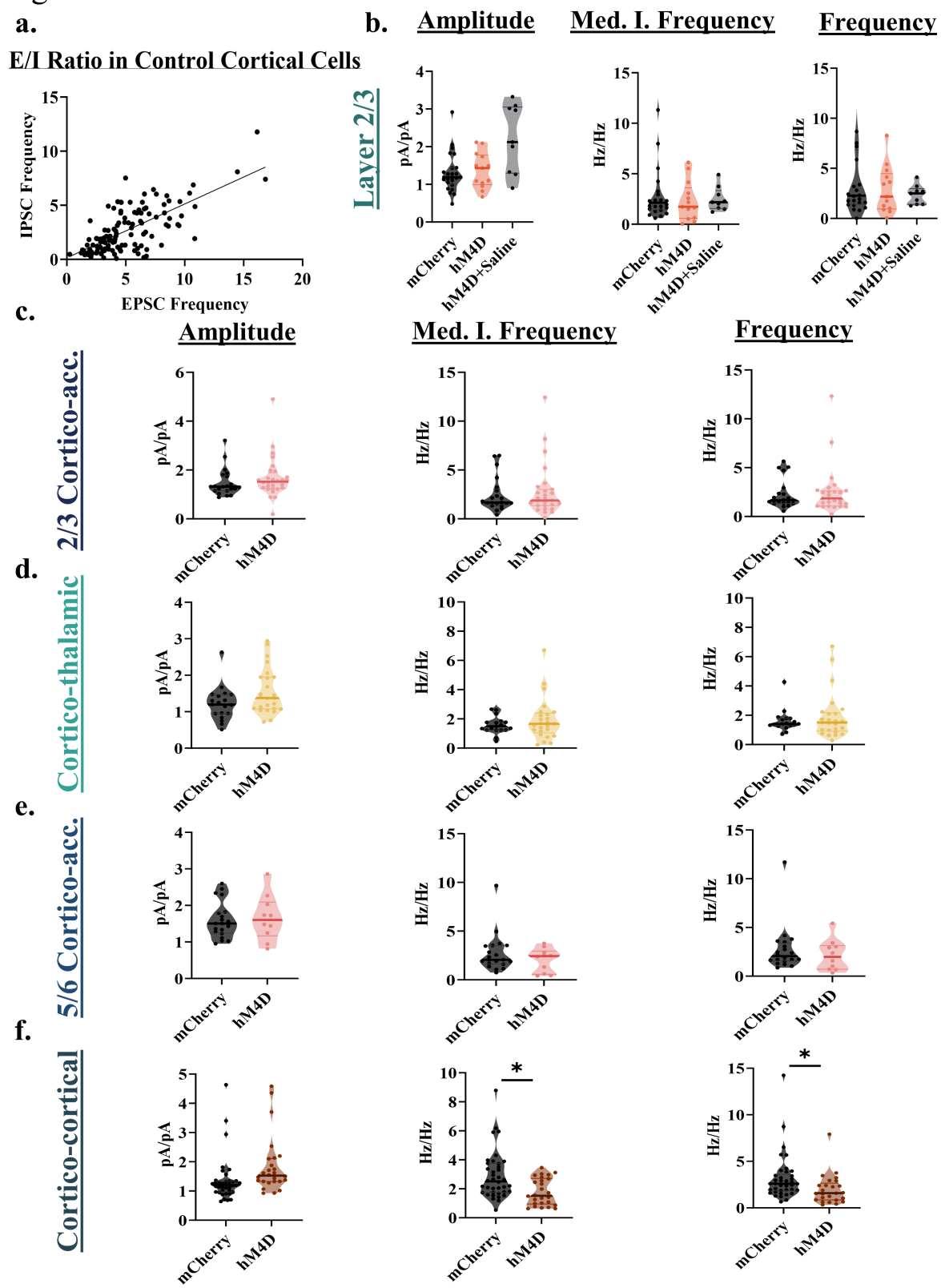
a.
E/I Ratio in Control Cortical Cells
IPSC Frequency
EPSC Frequency
b.
Amplitude
Med. I. Frequency
Frequency
Layer 2/3
pA/pA
Hz/Hz
mCherry
hM4D
hM4D+Saline
c.
Amplitude
Med. I. Frequency
Frequency
2/3 Cortico-acc.
d.
Cortico-thalamic
e.
5/6 Cortico-acc.
f.
Cortico-cortical
*

Figure 6) Adolescent thalamocortical inhibition disrupts E/I Ratio in cortical projecting cortical cells. a, Excitatory to inhibitory regression in control cortical cells. There was a significant correlation between EPSCs and IPSCs [R^2=0.4935, d.f. =1,121, P<0.0001]. **b**, Excitatory/Inhibitory ratio in nonspecific layer II/III cells for amplitude (left), median instantaneous frequency (middle), and frequency (right). There was no significant difference in E/I ratio between mCherry 1.188(0.400) pA/pA, hM4D 1.432(0.704) pA/pA or hM4D+Saline 2.005(1.247) pA/pA for amplitude [f = 2.567, d.f. = 2, 11.07 P = 0.121]. There was no significant difference in E/I ratio between mCherry 2.131(2.020) Hz/Hz, hM4D 1.736(2.409) Hz/Hz or hM4D+Saline 2.183(1.306) Hz/Hz for median instantaneous frequency [f = 0.713, d.f. = 2, 11.65 P = 0.511]. There was no significant difference in E/I ratio between mCherry 2.265(4.677) Hz/Hz, hM4D 2.186(3.134) Hz/Hz or hM4D+Saline 2.490(1.325) Hz/Hz for median instantaneous frequency [f = 1.209, d.f. = 2, 43 P = 0.308]. **c**, Excitatory/Inhibitory ratio in layer II/III accumbens projecting cortical cells for amplitude (left), median instantaneous frequency (middle), and frequency (right). There was no significant difference in E/I ratio between mCherry 1.316(0.587) pA/pA or hM4D 1.524(0.505) pA/pA for amplitude [f = 0.543, d.f. = 1, 6.59 P = 0.487]. There was no significant difference in E/I ratio between mCherry 1.686(1.368) Hz/Hz and hM4D 1.999(1.715) Hz/Hz for median instantaneous frequency [f = 0.836, d.f. = 1, 7.91 P = 0.388]. There was no significant difference in E/I ratio between mCherry 1.663(0.963) Hz/Hz and hM4D 1.865(1.406) Hz/Hz for frequency [f = 0.750, d.f. = 1, 8.10 P = 0.411]. **d**, Excitatory/Inhibitory ratio in layer V/VI thalamic projecting cortical cells for amplitude (left), median instantaneous frequency (middle), and frequency (right). There was no significant difference in E/I ratio between mCherry 1.195(0.500) pA/pA or hM4D 1.376(0.858) pA/pA for amplitude [f = 3.625, d.f. = 1, 42 P = 0.064]. There was no significant difference in E/I ratio between mCherry 1.414(0.485) Hz/Hz and hM4D 1.660(1.143) Hz/Hz for median instantaneous frequency [f = 0.975, d.f. = 1, 5.21 P = 0.367]. There was no significant difference in E/I ratio between mCherry 1.414(0.485) Hz/Hz and hM4D 1.503(1.136) Hz/Hz for frequency [f = 1.115, d.f. = 1, 5.31 P = 0.337]. **e**, Excitatory/Inhibitory ratio in layer V/VI accumbens projecting cortical cells for amplitude (left), median instantaneous frequency (middle), and frequency (right). There was no significant difference in E/I ratio between mCherry 1.467(0.624) pA/pA or hM4D 1.730(0.618) pA/pA for amplitude [f = 2.220, d.f. = 1, 28 P = 0.147]. There was no significant difference in E/I ratio between mCherry 2.060(1.840) Hz/Hz and hM4D 2.432(1.435) Hz/Hz for median instantaneous frequency [f = 0.412, d.f. = 1, 12.33 P = 0.533]. There was no significant difference in E/I ratio between mCherry 1.829(1.623) Hz/Hz and hM4D 2.658(1.765) Hz/Hz for frequency [f = 0.014, d.f. = 1, 12.10 P = 0.908]. **f**, Excitatory/Inhibitory ratio in cortical projecting cortical cells for amplitude (left), median instantaneous frequency (middle), and frequency (right). There was no significant difference in E/I ratio between mCherry 1.209(0.359) pA/pA or hM4D 1.473(0.403) pA/pA for amplitude [f = 1.099, d.f. = 1, 59 P = 0.299]. There was a significant decrease in E/I ratio between mCherry 2.513(1.915) Hz/Hz and hM4D 1.517(1.670) Hz/Hz for median instantaneous frequency. There was

also a significant decrease in E/I ratio between mCherry 2.594(1.607) Hz/Hz and hM4D 1.564(1.544) Hz/Hz for frequency. All reported values are Median(Interquartile Range). *P<0.05.

between mCherry 2.594(1.607) Hz/Hz and hM4D 1.564(1.544) Hz/Hz for frequency. All reported values are Median(Interquartile Range). *P<0.05.

492

Sup. Figure 1.

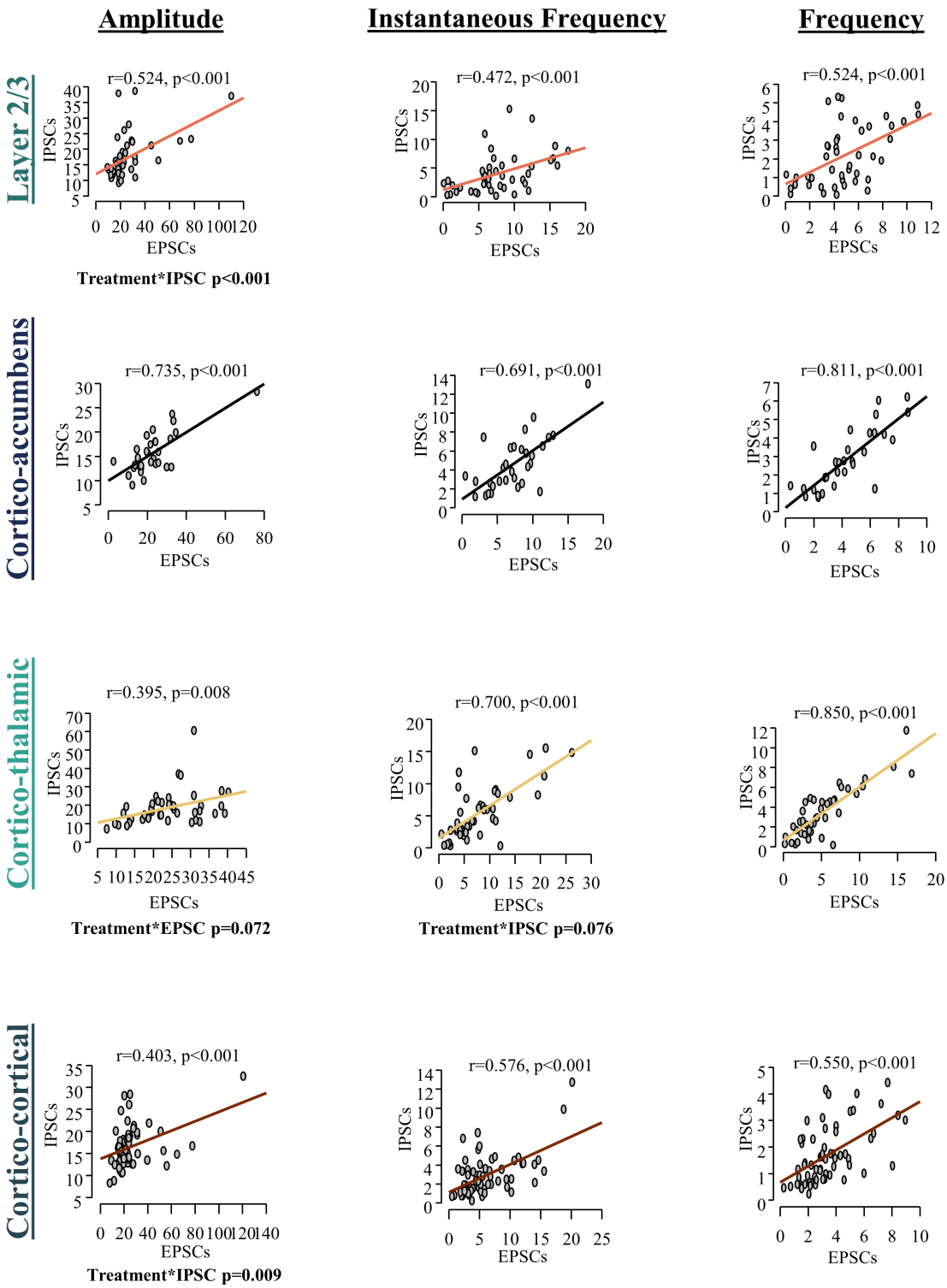
Amplitude
Instantaneous Frequency
Frequency
Layer 2/3
r=0.524, p<0.001
r=0.472, p<0.001
r=0.524, p<0.001
Treatment*IPSC p<0.001
Cortico-accumbens
r=0.735, p<0.001
r=0.691, p<0.001
r=0.811, p<0.001
Cortico-thalamic
r=0.395, p=0.008
r=0.700, p<0.001
r=0.850, p<0.001
Treatment*EPSC p=0.072
Treatment*IPSC p=0.076
Cortico-cortical
r=0.403, p<0.001
r=0.576, p<0.001
r=0.550, p<0.001
Treatment*IPSC p=0.009
IPSCs
EPSCs

Supplementary Figure 1) Regression analyses for E/I Ratio across all experiments.

Sup. Figure 2.

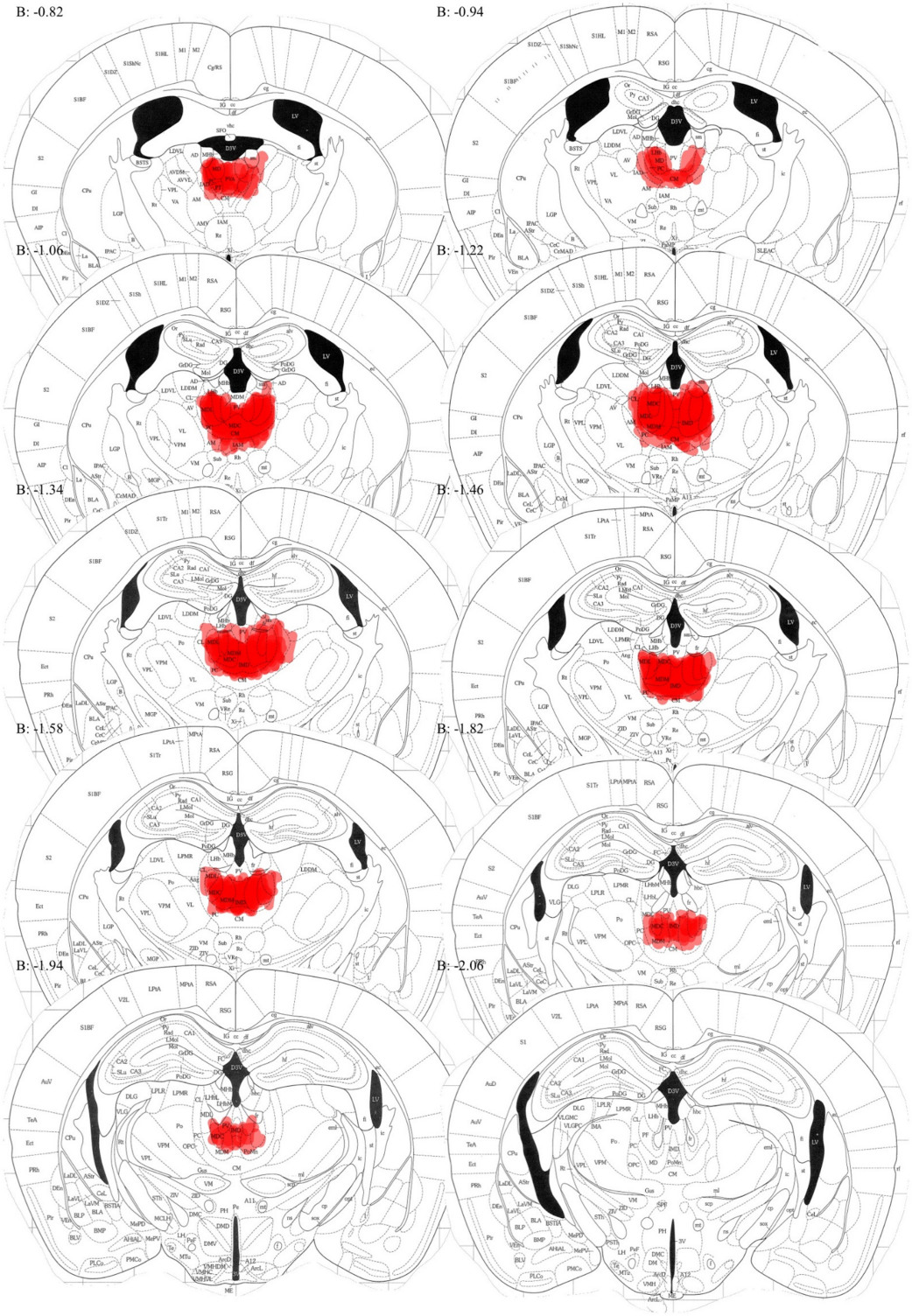

Supplementary Figure 2) Total viral spread of hM4D-mCherry Receptor in Red. B is distance from bregma.

493

494 **References**

495 Ahrlund-Richter S, Xuan Y, van Lunteren JA, Kim H, Ortiz C, Pollak Dorocic I, Meletis K,
496 Carlen M (2019) A whole-brain atlas of monosynaptic input targeting four different cell
497 types in the medial prefrontal cortex of the mouse. Nature neuroscience 22:657-668.
498 Anastasiades PG, Carter AG (2021) Circuit organization of the rodent medial prefrontal cortex.
499 Trends in neurosciences 44:550-563.
500 Anastasiades PG, Marlin JJ, Carter AG (2018) Cell-Type Specificity of Callosally Evoked
501 Excitation and Feedforward Inhibition in the Prefrontal Cortex. Cell reports 22:679-692.
502 Benoit LJ, Canetta S, Kellendonk C (2022a) Thalamocortical Development: A
503 Neurodevelopmental Framework for Schizophrenia. Biological psychiatry.
504 Benoit LJ, Holt ES, Posani L, Fusi S, Harris AZ, Canetta S, Kellendonk C (2022b) Adolescent
505 thalamic inhibition leads to long-lasting impairments in prefrontal cortex function. Nature
506 neuroscience 25:714-725.
507 Bhattacherjee A, Djekidel MN, Chen R, Chen W, Tuesta LM, Zhang Y (2019) Cell type-specific
508 transcriptional programs in mouse prefrontal cortex during adolescence and addiction.
509 Nature communications 10:4169.
510 Bonaventura J et al. (2019) High-potency ligands for DREADD imaging and activation in
511 rodents and monkeys. Nature communications 10:4627.
512 Canetta S, Teboul E, Holt E, Bolkan SS, Padilla-Coreano N, Gordon JA, Harrison NL,
513 Kellendonk C (2020) Differential Synaptic Dynamics and Circuit Connectivity of
514 Hippocampal and Thalamic Inputs to the Prefrontal Cortex. Cereb Cortex Commun
515 1:tgaa084.
516 Chini M, Hanganu-Opatz IL (2021) Prefrontal Cortex Development in Health and Disease:
517 Lessons from Rodents and Humans. Trends in neurosciences 44:227-240.
518 Cho KKA, Shi J, Phensy AJ, Turner ML, Sohal VS (2023) Long-range inhibition synchronizes
519 and updates prefrontal task activity. Nature 617:548-554.
520 Collins DP, Anastasiades PG, Marlin JJ, Carter AG (2018) Reciprocal Circuits Linking the
521 Prefrontal Cortex with Dorsal and Ventral Thalamic Nuclei. Neuron 98:366-379 e364.
522 Delevich K, Tucciarone J, Huang ZJ, Li B (2015) The Mediodorsal Thalamus Drives
523 Feedforward Inhibition in the Anterior Cingulate Cortex via Parvalbumin Interneurons.
524 The Journal of neuroscience : the official journal of the Society for Neuroscience
525 35:5743-5753.
526 Dienel SJ, Schoonover KE, Lewis DA (2022) Cognitive Dysfunction and Prefrontal Cortical
527 Circuit Alterations in Schizophrenia: Developmental Trajectories. Biological psychiatry
528 92:450-459.
529 Feinberg I (1982) Schizophrenia: caused by a fault in programmed synaptic elimination during
530 adolescence? Journal of psychiatric research 17:319-334.
531 Fuster JM (2001) The prefrontal cortex--an update: time is of the essence. Neuron 30:319-333.

532 Gogtay N, Vyas NS, Testa R, Wood SJ, Pantelis C (2011) Age of onset of schizophrenia:
533 perspectives from structural neuroimaging studies. Schizophrenia bulletin 37:504-513.
534 Hasegawa I, Fukushima T, Ihara T, Miyashita Y (1998) Callosal window between prefrontal
535 cortices: cognitive interaction to retrieve long-term memory. Science 281:814-818.
536 Holler-Wallscheid MS, Thier P, Pomper JK, Lindner A (2017) Bilateral recruitment of prefrontal
537 cortex in working memory is associated with task demand but not with age. Proceedings
538 of the National Academy of Sciences of the United States of America 114:E830-E839.
539 Kalivas PW, Volkow N, Seamans J (2005) Unmanageable motivation in addiction: a pathology in
540 prefrontal-accumbens glutamate transmission. Neuron 45:647-650.
541 Mannella F, Gurney K, Baldassarre G (2013) The nucleus accumbens as a nexus between values
542 and goals in goal-directed behavior: a review and a new hypothesis. Frontiers in
543 behavioral neuroscience 7:135.
544 Manvich DF, Webster KA, Foster SL, Farrell MS, Ritchie JC, Porter JH, Weinshenker D (2018)
545 The DREADD agonist clozapine N-oxide (CNO) is reverse-metabolized to clozapine and
546 produces clozapine-like interoceptive stimulus effects in rats and mice. Scientific reports
547 8:3840.
548 McGlinchey EM, James MH, Mahler SV, Pantazis C, Aston-Jones G (2016) Prelimbic to
549 Accumbens Core Pathway Is Recruited in a Dopamine-Dependent Manner to Drive Cued
550 Reinstatement of Cocaine Seeking. The Journal of neuroscience : the official journal of
551 the Society for Neuroscience 36:8700-8711.
552 Miller EK, Lundqvist M, Bastos AM (2018) Working Memory 2.0. Neuron 100:463-475.
553 Nabel EM, Morishita H (2013) Regulating critical period plasticity: insight from the visual
554 system to fear circuitry for therapeutic interventions. Front Psychiatry 4:146.
555 Nabel EM, Garkun Y, Koike H, Sadahiro M, Liang A, Norman KJ, Taccheri G, Demars MP, Im
556 S, Caro K, Lopez S, Bateh J, Hof PR, Clem RL, Morishita H (2020) Adolescent frontal
557 top-down neurons receive heightened local drive to establish adult attentional behavior in
558 mice. Nature communications 11:3983.
559 Paus T, Keshavan M, Giedd JN (2008) Why do many psychiatric disorders emerge during
560 adolescence? Nature reviews Neuroscience 9:947-957.
561 Rapoport JL, Giedd JN, Gogtay N (2012) Neurodevelopmental model of schizophrenia: update
562 2012. Molecular psychiatry 17:1228-1238.
563 Sakurai T, Gamo NJ (2019) Cognitive functions associated with developing prefrontal cortex
564 during adolescence and developmental neuropsychiatric disorders. Neurobiology of
565 Disease 131:104322.
566 Smucny J, Dienel SJ, Lewis DA, Carter CS (2022) Mechanisms underlying dorsolateral
567 prefrontal cortex contributions to cognitive dysfunction in schizophrenia.
568 Neuropsychopharmacology : official publication of the American College of
569 Neuropsychopharmacology 47:292-308.
570 Sun Q, Li X, Ren M, Zhao M, Zhong Q, Ren Y, Luo P, Ni H, Zhang X, Zhang C, Yuan J, Li A,
571 Luo M, Gong H, Luo Q (2019) A whole-brain map of long-range inputs to GABAergic
572 interneurons in the mouse medial prefrontal cortex. Nature neuroscience 22:1357-1370.
573 Weinberger DR (1987) Implications of normal brain development for the pathogenesis of
574 schizophrenia. Archives of general psychiatry 44:660-669.
575 Wen W, Turrigiano GG (2021) Developmental Regulation of Homeostatic Plasticity in Mouse
576 Primary Visual Cortex. The Journal of neuroscience : the official journal of the Society
577 for Neuroscience 41:9891-9905.

578 Wiesel TN, Hubel DH (1963) Single-Cell Responses in Striate Cortex of Kittens Deprived of
579 Vision in One Eye. Journal of neurophysiology 26:1003-1017.
580 Yang SS, Mack NR, Shu Y, Gao WJ (2021) Prefrontal GABAergic Interneurons Gate Long-
581 Range Afferents to Regulate Prefrontal Cortex-Associated Complex Behaviors. Frontiers
582 in neural circuits 15:716408.
583